Volume 53
Number 17
7 May 2024
Pages 7243-7644

Dalton Transactions

An international journal of inorganic chemistry

rsc.li/dalton

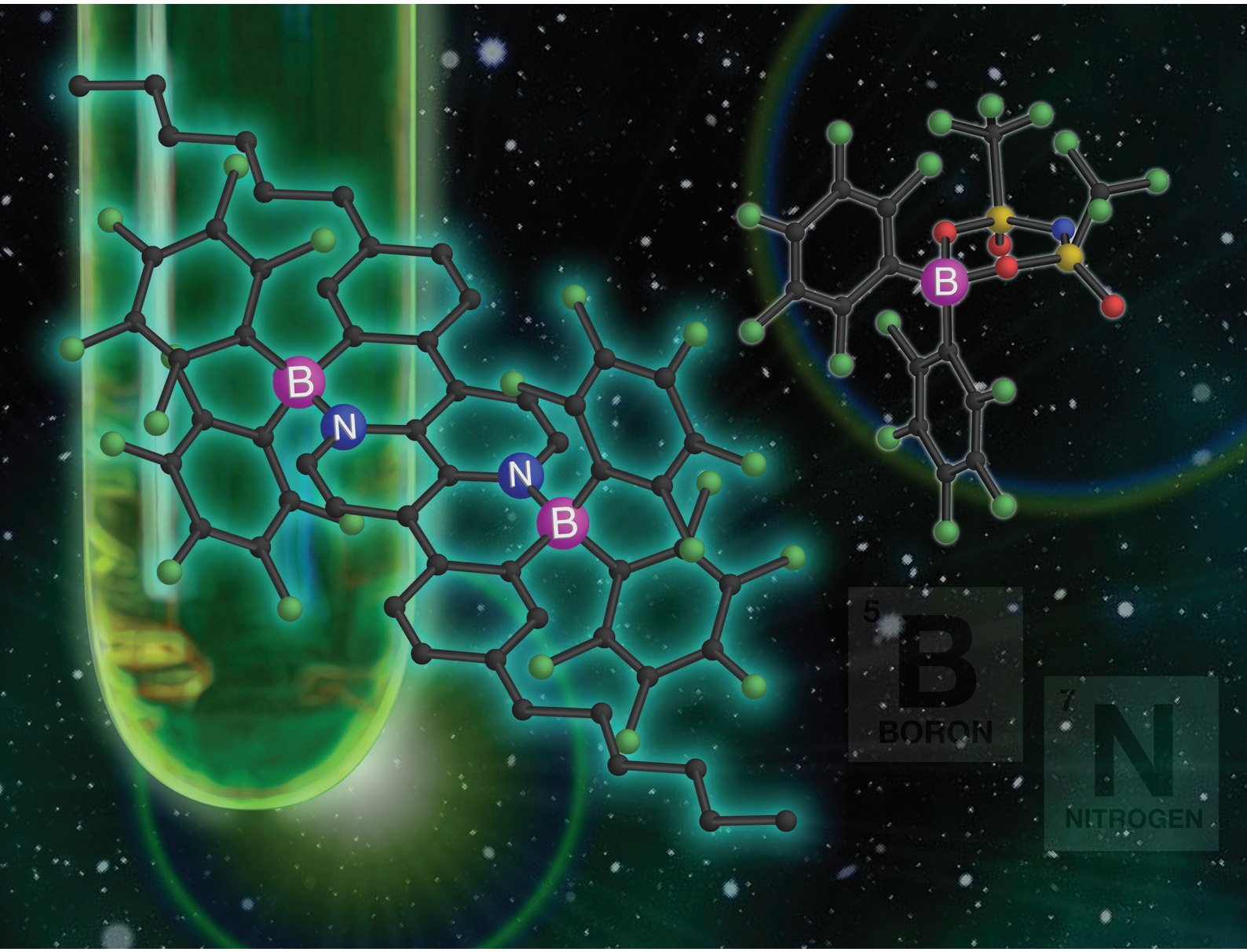

ISSN 1477-9226

ROYAL SOCIETY OF CHEMISTRY

PAPER

Warren E. Piers *et al.*

Direct C–H electrophilic borylation with $(C_6F_5)_2B–NTf_2$ to generate B–N dibenzo[*a*,*h*]pyrenes

Dalton Transactions

ROYAL SOCIETY OF CHEMISTRY

PAPER

View Article Online
View Journal | View Issue

Cite this: *Dalton Trans.*, 2024, **53**, 7273

Direct C–H electrophilic borylation with $(C_6F_5)_2B–NTf_2$ to generate B–N dibenzo[*a*,*h*]pyrenes†

Tony Nguyen,[a] Jason L. Dutton,[a,b] Chia Yun Chang,[a] Wen Zhou[a] and Warren E. Piers *[a]

Received 17th February 2024,
Accepted 7th March 2024

DOI: 10.1039/d4dt00469h

rsc.li/dalton

The borylation of aryl substituted pyridines is an effective way of preparing B–N doped conjugated organic frameworks. Trihaloborane Lewis acids are often employed for this protocol, and may require further functionalization to replace the remaining halides on boron. We report a new, fully characterized, electrophilic borylating agent, $(C_6F_5)_2B(\kappa^2\text{-}NTf_2)$, that smoothly incorporates a $-B(C_6F_5)_2$ unit into the model substrate 2-phenylpyridine. To demonstrate its utility in preparing more complex B–N doped structures, we use it to prepare seven examples of the 6a,13a-diaza-7,14-dibora-dibenzo[*a*,*h*]pyrene framework, with substituents of varying donor properties. The structural, redox, and photophysical properties of this new family of B–N doped polycyclic hydrocarbon compounds were probed experimentally and computationally.

Introduction

The strategy of substituting C–C units in conjugated organic materials with isoelectronic, isosteric B–N building blocks as a means of modifying the photophysical and redox properties of a given molecular material has been a topic of widespread study in the past 15 years. While initial studies from Dewar[1–7] laid the early groundwork for this concept, our 2007 report of 10a-aza-10b-borapyrene[8,9] (**I**, Chart 1) helped initiate a modern era of "BN for CC"[10] development of new materials, polymers, biologically active molecules and novel ligands utilizing this concept.[11–22]

In the context of conducting or semiconducting organic materials, the incorporation of B–N units can utilize three coordinate, planar boron centers or four coordinate tetrahedral geometries at boron. Select examples of each are given in Chart 1 (planar, **I**,[8] **II**,[23] **III**,[24] **IV**;[25] tetrahedral **V**,[26] **VI**,[27] **VII**[28]). Incorporation of planar boron centers potentially allows for more effective conjugation in the core framework but these materials can be more reactive towards Lewis bases, reducing agents, and O_2 (for example *via* Diels–Alder type additions).[29] These planar materials can also be generally less soluble/processable due to favorable π stacking interactions in the solid state. Tetrahedral boron centers can disrupt these intermolecular interactions to some degree but may lead to less favorable redox properties due to higher LUMO energy levels. However, such materials tend to be more stable under ambient conditions and are therefore easier to prepare and handle, not requiring any special conditions for use in applications requiring device preparation.[30,31]

In either type of system, efficient synthesis for preparation of these molecules at scale remains challenging.[16] For preparation of molecules like **VI** and **VII**, intramolecular, directed electrophilic C–H borylation is a powerful method for introducing B–N units when the directing group is a nitrogenous base.[21] Building on seminal work from Vedejs and coworkers,[32] Murakami,[33] Wang[34] and Ingleson[35] have utilized this approach effectively on phenyl pyridine substrates to prepare a variety of B–N indene and fluorene heterocycles with tetrahedral boron centers under mild conditions. The most common borylating agents here are the Lewis acidic trihalides BX_3 (X = Cl, Br) and necessarily produce tetrahedral BX_2 centers in the products. While the rigid chelate effectively prevents decoordination of the nitrogen, in polar media the halides can be labile, producing borenium cations[36,37] that are susceptible to hydrolysis or ligation by Lewis bases. This becomes more facile upon one or two electron reduction. Often, then, these $(BX_2)_n$ compounds are functionalized with aryl or alkyl units *via* some sort of transmetallation step which, depending on the number of BX_2 units in the framework, can be low yielding and/or unselective. Further, in some instances (as shown herein specifically) the BX_2 derivatives can

[a]*Department of Chemistry, University of Calgary, 2500 University Drive NW, Calgary, Alberta T2N 1N4, Canada. E-mail: wpiers@ucalgary.ca*
[b]*Department of Biochemistry and Chemistry, La Trobe Institute for Molecular Science, La Trobe University, Melbourne, Victoria 3086, Australia*

†Electronic supplementary information (ESI) available: General experimental details, synthesis and characterization of all new compounds, NMR studies and computation data files, see end of document. CCDC 2333166–2333175. For ESI and crystallographic data in CIF or other electronic format see DOI: https://doi.org/10.1039/d4dt00469h

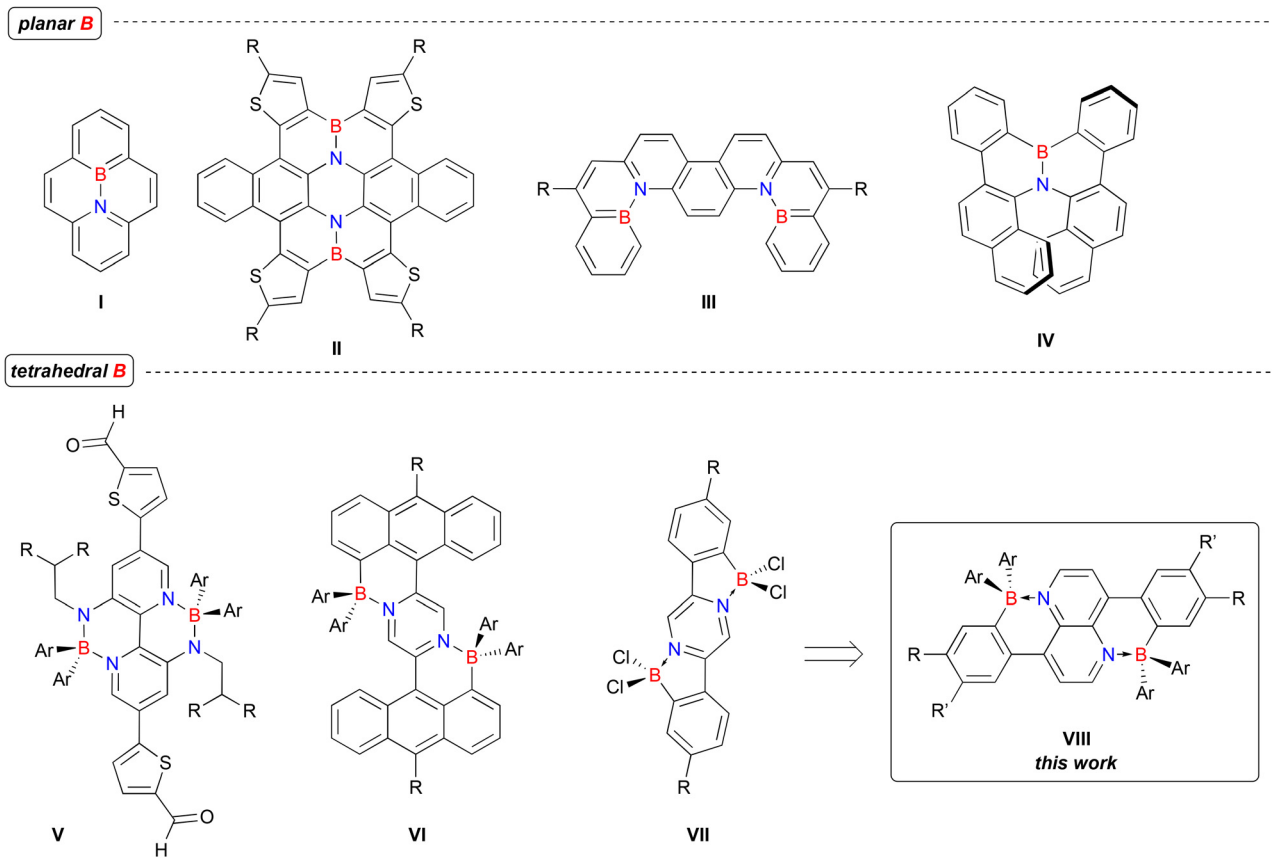

Chart 1 Notable examples of B–N doped polycyclic aromatic hydrocarbons.

be poorly soluble, making multiple borylations and functionalization *via* transmetallation more synthetically challenging.

Against this backdrop, we report here the synthesis of a number of examples of a new family of conjugated BN-dibenzo[*a*,*h*]pyrenes (**VIII**, Chart 1) incorporating $-B(C_6F_5)_2$ centers in the framework, along with their structures, and photophysical and redox properties. To avoid the intermediacy of BX_2 derivatives, we introduce a new electrophilic borylating agent incorporating the triflimide group,[38] **$(C_6F_5)_2BNTf_2$**. This weakly coordinating anion can loosely chelate Lewis acidic centers[38,39] while remaining highly labile and we demonstrate that **$(C_6F_5)_2BNTf_2$** is an effective electrophilic borylating agent that directly gives the target $-B(C_6F_5)_2$ products without the need for a transmetallation step.

Results and discussion

Directed borylation of aryl C–H bonds adjacent to pyridyl or related nitrogenous functions is an excellent methodology for preparing B–N containing units within larger conjugated systems. Typically, haloboranes BX_3 are employed, furnishing dihalo B–N compounds that require further functionalization to install alkyl or aryl groups on boron; these BX_2 derivatives can exhibit poor solubility, which hampers multiple borylations and/or renders the subsequent transmetallation steps difficult. We were therefore interested in instituting $-B(C_6F_5)_2$ units directly and attempted borylation of 2-phenylpyridine (**PhPy**) as a model substrate using the chloroborane $(C_6F_5)_2BCl$.[40,41] This substrate was chosen, since the B,N fluorene product (compound **IX**, Scheme 2 below) is known.[33,42] Using the bulky base 2,6-di-*tert*-butyl-pyridine (**DTBP**) to scavenge HCl, this reaction proved unsuccessful, where only trace amounts of the product was formed (5% NMR yield) even with extensive heating for 16 hours. The remaining 95% of the 2-phenylpyridine appears to be tied up as the B ← N Lewis pair between $(C_6F_5)_2BCl$ and **PhPy** (Fig. S1 and S2†). Addition of $AlCl_3$ to activate the chloroborane[35] led to product formation, but for more functional group tolerance and a simpler reaction protocol, we sought a "preactivated" borylation reagent for $-B(C_6F_5)_2$ groups and prepared the triflato and triflimato compounds **$(C_6F_5)_2BOTf$** and **$(C_6F_5)_2BNTf_2$** through treatment of $(C_6F_5)_2BCl$ with the appropriate $TMSETf_n$ reagent (TMS = trimethylsilyl; E = O, N; Tf = $-SO_2CF_3$ and n = 1, 2) as shown in Scheme 1. These reactions proceed smoothly at room temperature in dichloromethane, delivering the two products in reasonable yields as white solids. The new reagents were fully characterized, including *via* X-ray crystallography (see the ESI† for full details, and Fig. 1). While the triflato complex is

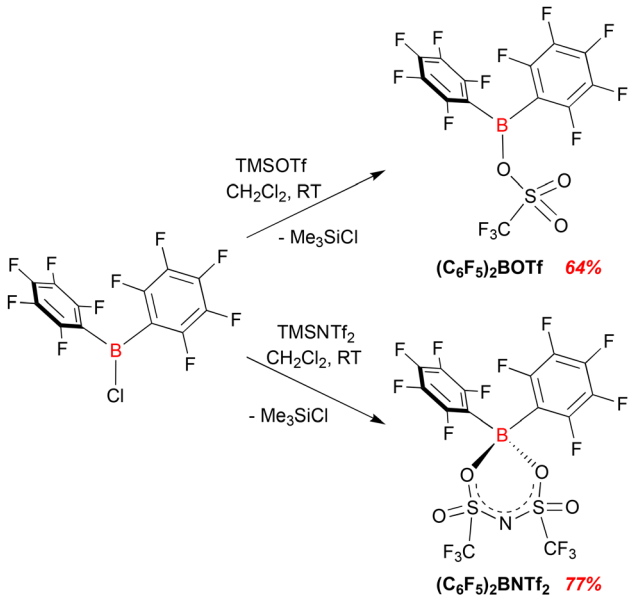

Scheme 1 Synthesis of $(C_6F_5)_2BOTf$ and $(C_6F_5)_2BNTf_2$.

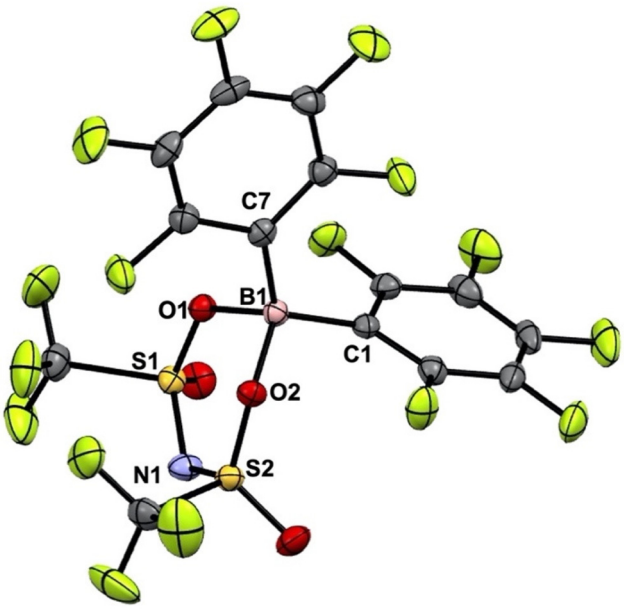

Fig. 1 Molecular structure of $(C_6F_5)_2BNTf_2$. Thermal ellipsoids drawn at 50% probability level. Selected bond lengths (Å) B(1)–O(1) 1.569(3), B(1)–O(2) 1.555(2), O(1)–S(1) 1.491(2), O(2)–S(2) 1.496(2), S(1)–N(1) 1.561(2), S(2)–N(1) 1.561(2). Selected bond angles (°): O(1)–B(1)–O(2), 102.33(13); C(1)–B(1)–C(7), 119.21(15).

effective in the reactions discussed below, it is not overly stable in solution, even at low temperatures, and in the solid state turns to a brown oily material when exposed to high vacuum, rendering it difficult to keep pure (Fig. S3–S6†). For this reason, we have primarily utilized the triflimato boryl reagent, since it is highly reactive and stable in the absence of moisture, and is easily handled as a white, microcrystalline solid. Its superior stability likely stems from the tetrahedral coordination about the boron center due to the κ^2 coordination of the NTf_2 anion (Fig. 1). The NTf_2 anion is readily displaced by 2,2′-bipyridine to form a boronium ion (by NMR spectroscopy), confirming the weakly coordinating, labile nature of this anion relative to chloride (Fig. S7 and S8†).[38]

Accordingly, reaction of $(C_6F_5)_2BNTf_2$ with the model substrate **PhPy** rapidly gives the product **IX**[33,42] in the presence of **DTBP** to remove the aryl C–H proton at the locus of borylation. Two sets of conditions were explored as shown in Scheme 2 and monitored in C_6D_5Br by multinuclear NMR spectroscopy at room temperature (Fig. S9–S12†). In the first (left side of Scheme 2), the substrate was mixed in a 1 : 1 ratio with $(C_6F_5)_2BNTf_2$ and an immediate reaction to form 0.5 equivalents of **IX** along with protonated **PhPy** was observed, suggesting the substrate itself is an effective Brønsted base in this reaction. Addition of **DTBP** to this mixture required extensive heating at 100 °C to eventually give ≈90% conversion to **IX** by NMR spectroscopy. We presume this is due to kinetic difficulties in transfer of the proton between these two bases since the thermodynamic basicity of **PhPy** is slightly lower than that of **DTBP** (pK_a [**PhPyH**]$^+$ = 4.48;[43] pK_a [**DTBPH**]$^+$ = 4.95[44]). Accordingly, when **DTBP** was added to $(C_6F_5)_2BNTf_2$, no reaction was observed, but subsequent dropwise addition of substrate **PhPy** resulted in immediate conversion to product, with loss of [**DTBPH**]$^+$[NTf_2]$^-$ byproduct (Scheme 2, right hand side). When substrate was added to the $(C_6F_5)_2BNTf_2$/**DTBP** mixture in 0.2 equivalent increments, stepwise conversion to products was observed, indicating a very clean, selective conversion at room temperature. While we have not conducted detailed mechanistic studies, the lack of observable intermediates in these experiments indicate that

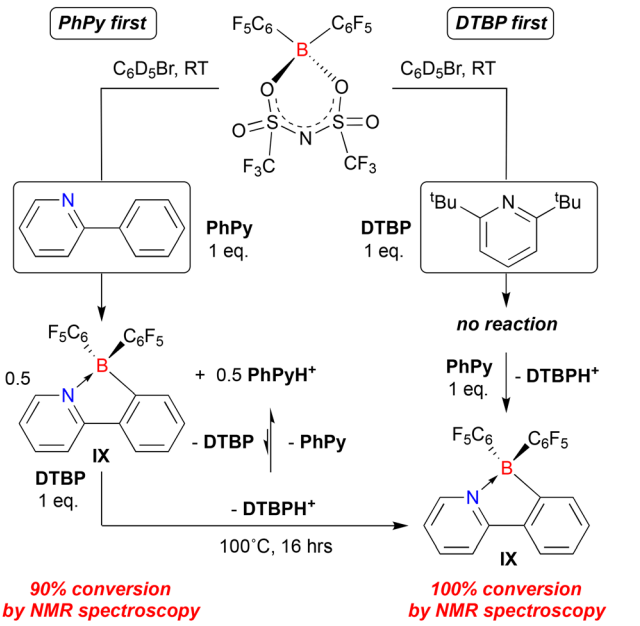

Scheme 2 Borylation of 2-phenylpyridine (**PhPy**) with $(C_6F_5)_2BNTf_2$.

the NTf_2 anion is readily displaced from boron by **PhPy** and the $(C_6F_5)_2BNTf_2$ reagent is an effective source of electrophilic $-B(C_6F_5)_2$.

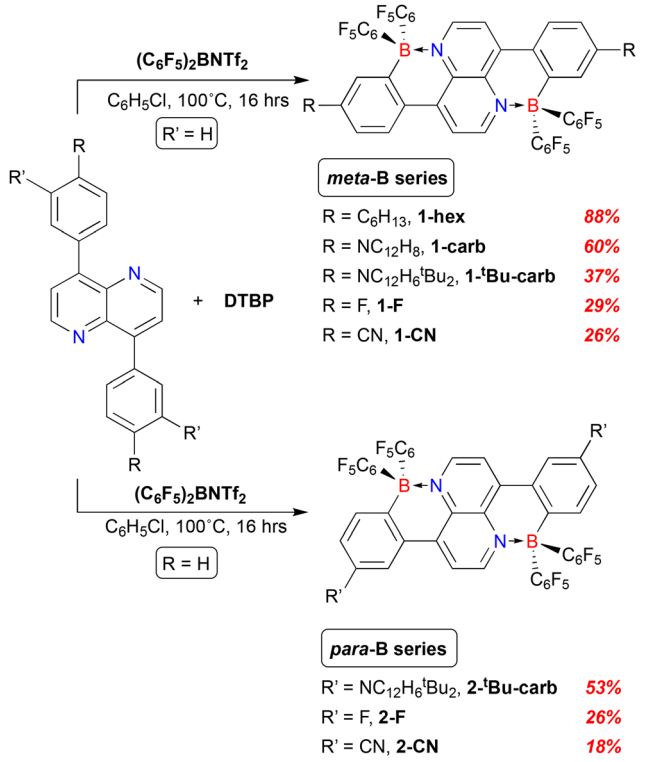

Scheme 3 Syntheses of 6a,13a-diaza-7,14-dibora-dibenzo[*a*,*h*]pyrenes.

With the methodology to directly install $-B(C_6F_5)_2$ units using directed borylation with the new reagent $(C_6F_5)_2BNTf_2$ in hand, we sought to use it to prepare a new family of conjugated BN doped polycyclic aromatic hydrocarbons. We chose to target B–N pyrene units with annulated benzene rings by borylating 4,8-diaryl-1,5-naphthyridines, which are readily prepared by C–C coupling reactions[45] starting from the dibromo-1,5-naphthyridine building block[46] (see ESI† for details). The products are BN analogs of the dibenzo[*a*,*h*]pyrene framework, albeit with a saturated, tetrahedral node at the 7,14 bora positions. The parent all carbon dibenzo[*a*,*h*]pyrene unit is related to the base structure of the commercially available orange dye Vat Orange 1, which has recently been incorporated into donor–acceptor π-conjugated polymers for use in organic electronic devices.[47] To our knowledge, no BN doped versions of this framework have been reported.

Initial borylations on 4,8-diaryl-1,5-naphthyridines using the Murakami[33] or Ingleson[35] methodology with BX_3 (X = Cl or Br) resulted in an immediate precipitation of an insoluble product when the substituents R′ = H and R = CH_3, ^{t}Bu, or hexyl (see Scheme 3 for positions of R′ and R). These products were not further characterized due to their high insolubility. In contrast, borylating a variety of these substrates with $(C_6F_5)_2BNTf_2$ resulted primarily in soluble diborylated products that were isolated and fully characterized (Scheme 3). The R substituents range from electron donating (carbazole, hexyl) to electron withdrawing (F, CN) and a series in which the substituent is in the *meta* position relative to the borylated carbon (compounds **1-R**) were compared with a smaller series where the group is in the position *para* to boron (compounds

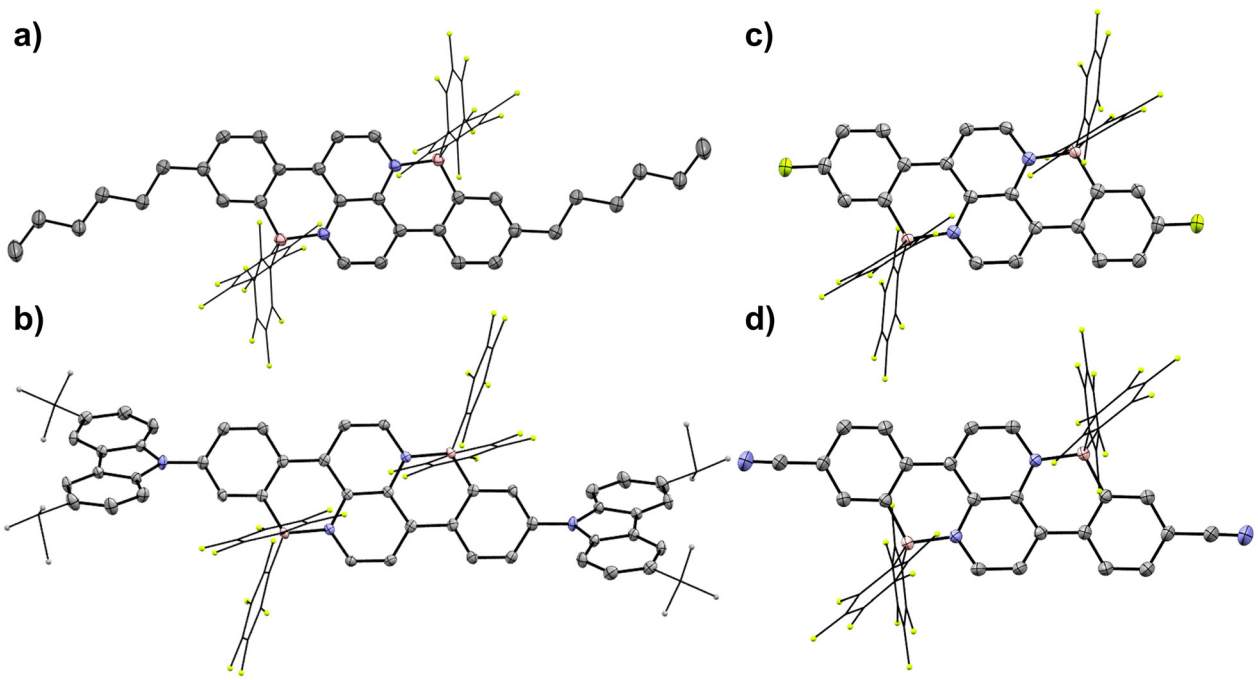

Fig. 2 Molecular structures of (a) **1-hex**, (b) **1-^{t}Bu-carb**, (c) **1-F**, and (d) **1-CN**. Hydrogen atoms and solvent have been omitted for clarity. C_6F_5 and ^{t}Bu groups are wireframe for clarity. Thermal ellipsoids drawn at 50% probability level. See Table 1 for selected metrical data.

2-R′). Isolated yields of the diborylated compounds range from good to poor and qualitatively correlate with the electron donating/withdrawing character of the R/R′ groups, with electron withdrawing groups giving poorer yields. In these systems, indications are that the other main products are the monoborylated compounds, the second borylation likely being discouraged by the lowered nucleophilicity of the remaining aryl group. Conditions required for these reactions were harsher than the model studies conducted with **PhPy** as described above because of the greater steric demands of this set of substrates, and there was no advantage to using a "**DTBP** first" protocol in these reactions. Finally, we note that the poor solubility of the derivative **1-carb** precluded its full spectral characterization, although its structure was determined by X-ray crystallography (see Fig. S13†). For this reason, the more soluble **1/2-^{t}Bu-carb** derivatives were prepared for comparative optoelectronic property studies. All the products of Scheme 3 are bench stable to air and moisture and have been fully characterized by multinuclear NMR spectroscopy, high-resolution mass spectrometry and X-ray crystallography.

Molecular structures for all the B–N dibenzo[*a*,*h*]pyrenes in Scheme 3 are shown in Fig. 2 (*meta*-B series) and Fig. 3 (*para*-B-series). Comparative selected metrical parameters are given in Table 1. Within the hexacyclic core, B–N bond distances are comparable to other similar compounds (*e.g.* Chart 1 [26–28]). The six conjugated rings are essentially planar, with a moderate twist engendered in some examples due to some flexibility in the dihedral angle defined by the four atoms in the structure's bay region (*i.e.*, C(3)–C(4)–C(5)–C(10), Table 1). This dihedral angle ranges from ≈1–15°, and as it gets larger, the B(1)

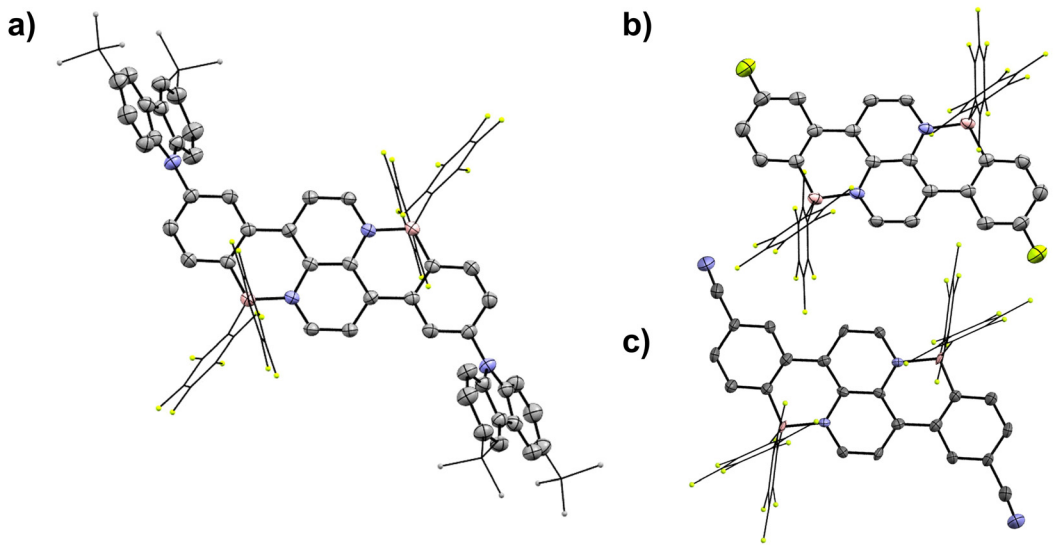

Fig. 3 Molecular structures of (a) **2-^{t}Bu-carb**, (b) **2-F**, and (c) **2-CN**. Hydrogen atoms, solvent, and disorder have been omitted for clarity. C_6F_5 groups and ^{t}Bu groups are wireframe for clarity. Thermal ellipsoids have been drawn at the 50% probability level. See Table 1 for selected metrical data.

Table 1 Selected metrical data for compounds **1-R** and **2-R′**

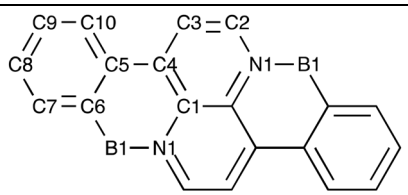

Compound	B(1)–N(1) (Å)	B(1)–C(6) (Å)	N(1)–C(1) (Å)	C(5)–C(4) (Å)	Bay dihedral[a] (°)	B(1) deviation[b] (Å)
1-hex	1.620(3)	1.597(4)	1.382(3)	1.471(3)	3.9(4)	0.12
1-^{t}Bu-carb	1.611(3)	1.618(4)	1.373(3)	1.455(4)	14.8(4)	0.39
1-F	1.608(3)	1.605(4)	1.376(3)	1.467(4)	1.0(3)	0.08
1-CN	1.623(3)	1.599(3)	1.380(2)	1.473(4)	9.7(3)	0.10
2-^{t}Bu-carb	1.628(3)	1.595(3)	1.380(3)	1.466(3)	13.6(3)	0.35
2-F	1.623(6)	1.610(5)	1.372(4)	1.477(6)	9.3(5)	0.07
2-CN	1.620(9)	1.600(9)	1.389(9)	1.470(1)	2.1(12)	0.04

[a] C(3)–C(4)–C(5)–C(10) dihedral angle. [b] Distance B(1) protrudes from plane defined by N(1)–C(1)–C(4)–C(5)–C(6).

Table 2 Summary of experimental photophysical and electronic data for compounds in both *meta*-B and *para*-B series

Compound	$\lambda_{abs}/(\varepsilon)$ nm/(M^{-1} cm^{-1})	$\lambda_{PL}/(\Phi_{PL})$ nm/(%)	Stokes shift (cm^{-1})	E_g^{opt} [a] (eV)	HOMO[b] (eV)	LUMO[b] (eV)	E_g^{elec} (eV)	E_{ox} [c] (V)	E_{red} [c] (V)
1-hex	467 (36 190)	489 (35)	963	2.48	—	−3.790	—	—	−0.986
1-F	448 (37 050)	469 (45)	999	2.58	—	−3.937	—	—	−0.863
2-F	433 (26 927)	522 (35)	3938	2.54	—	−4.082	—	—	−0.800
1-CN	413 (1920)	486 (3)	3637	2.68	—	−4.14	—	—	−0.660
2-CN	410 (9211)	482 (8)	3643	2.63	—	−4.11	—	—	−0.695
1-^{t}Bu-carb	611, 377 (22 069, 21 273)	Not emissive	—	1.68	−5.537	−3.896	1.641	0.820	−0.904
2-^{t}Bu-carb	432, 570 (22 846, 1645)	Not emissive	—	1.67	−5.587	−3.982	1.605	0.787	−0.818

[a] Wavelengths of the onset of absorption maxima were used to estimate the optical bandgap. [b] The potentials of E_{ox} and E_{red} were used to calculate the electrochemical HOMO and LUMO energy levels using the following equations: $E_{HOMO} = -(4.8 - E_{ox})$ or $E_{LUMO} = -(4.8 + E_{red})$, respectively. [c] E_{ox} and E_{red} were determined by calculating the $E_{1/2}$ of each oxidation and reduction event in the CVs.

atom deviates from the plane defined by the remaining five atoms in the boracyclic ring, creating a twist in the hexacyclic core. The twist is largest for the ^{t}Bu-carb substituted derivatives and there is no discernable correlation with the electronic properties of the substituents, so likely this feature is due primarily to packing forces. The C_6F_5 groups in the derivative with the largest dihedral angle (**1-^{t}Bu-carb**) remain equivalent at all temperatures in the ^{19}F NMR spectrum indicating an equilibrium planar structure in solution.

The redox and photophysical properties of the various B–N dibenzo[*a*,*h*]pyrenes were probed by cyclic voltammetry (to estimate the LUMO energies), absorption and photoluminescence spectroscopy (to estimate the HOMO–LUMO gap); the data is summarized in Table 2. In general, as for other BN doped polycyclic aromatic structures, DFT analysis indicates that the HOMO and LUMO energies are both stabilized relative to identical all carbon frameworks, while the HOMO–LUMO gaps similar between BN/CC congeners (see Fig. S14†). The BN doped compounds are therefore more easily reduced than their all-carbon analogs. This is borne out in the observed electrochemistry; B–N dibenzo[*a*,*h*]pyrenes here undergo reversible one-electron reductions at moderately negative potentials (Table 2, Fig. 4 and 5). As seen in Fig. 4, compound **1-hex**, **1-F**, and **1-CN** are reduced at progressively less negative potentials as the substituent becomes more electron withdrawing; a similar trend is seen for the *para*-B series **2-F** and **2-CN**.

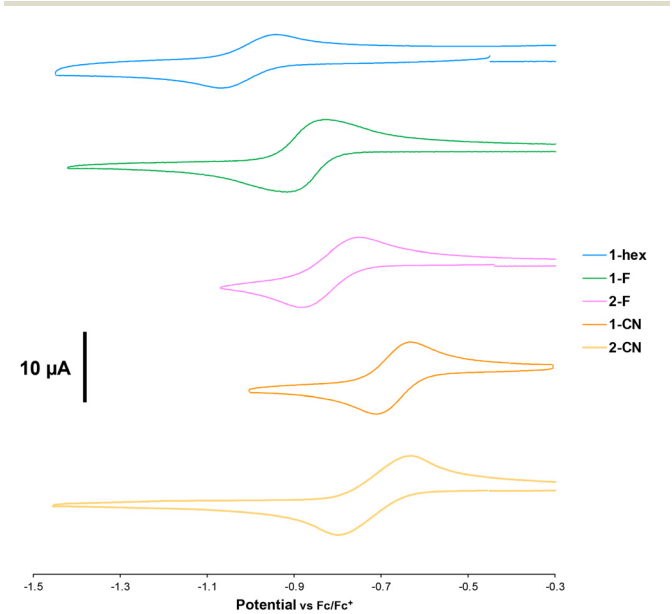

Fig. 4 Cyclic voltammograms of **1-hex** (blue), **1-F** (green), **2-F** (pink), **2-CN** (orange), and **2-CN** (yellow). CVs were recorded in THF solution with 0.1 M nBu$_4$PF$_6$ as supporting electrolyte at a scan rate of 100 mV s^{-1}, using a three-electrode setup with glassy carbon, Pt mesh, and Ag/AgCl, working, counter, and reference electrodes, respectively.

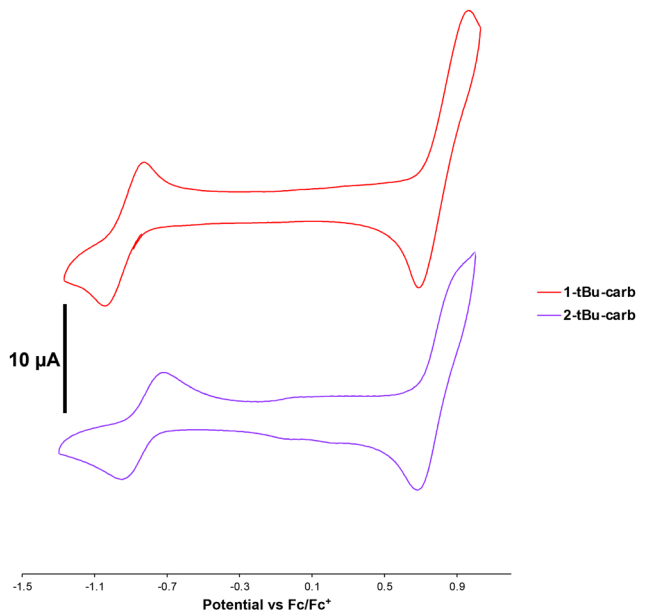

Fig. 5 Cyclic voltammograms of **1-^{t}Bu-carb** (red) and **2-^{t}Bu-carb** (purple). CVs were recorded in THF solution with 0.1 M nBu$_4$PF$_6$ as supporting electrolyte at a scan rate of 100 mV s^{-1}, using a three-electrode setup with glassy carbon, Pt mesh, and Ag/AgCl, working, counter, and reference electrodes, respectively.

This is indicative of the LUMO lowering in energy as the substituent becomes more electron withdrawing. For these compounds, no oxidation wave is observed upon scanning to the solvent limit, speaking to the oxidative stability of the B–N dibenzo[*a*,*h*]pyrene core. The compounds substituted with the ^{t}Bu-carbazole group also exhibit one electron reductions (Fig. 5) at potentials nearer to those observed for **1**/**2-F** than that of **1-hex**, suggesting that the carbazole group is functioning as an inductively withdrawing group in this instance. This is consistent with the observed structures (Fig. 2 and 3), in which the ^{t}Bu-carb group is essentially perpendicular to the hexacyclic core, and therefore out of conjugation with the B–N dibenzo[*a*,*h*]pyrene π system. As for the other examples, the reduction potential for **2-^{t}Bu-carb** is slightly anodically shifted in comparison to the *meta*-B derivative **1-^{t}Bu-carb**. Furthermore, as seen in the CV traces in Fig. 5, these carbazole substituted examples do exhibit an oxidation wave at around 0.8 V, due to removal of an electron from the carbazole nitrogen.[48]

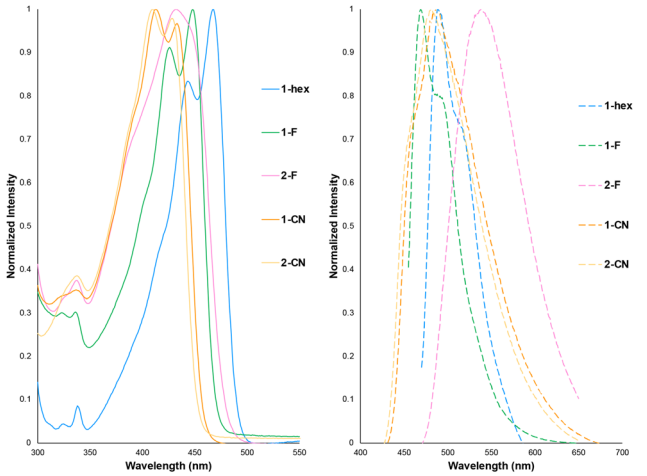

Fig. 6 The normalized absorption (left) and photoluminescent (right) spectra of **1-hex** (blue), **1-F** (green), **2-F** (pink), **2-CN** (orange), and **2-CN** (yellow). Optical absorption and photoluminescent spectra were recorded in 10^{-5} M solutions in DCM.

The normalized optical absorption and photoluminescence spectra for compounds **1-hex**, **1-F**, **2-F**, **1-CN**, and **2-CN** are shown in Fig. 6 and the absorption and emission data are given in Table 2. All of these derivatives exhibit π → π* transitions in the 410–467 nm range, with more electron withdrawing groups inducing higher energy absorptions. Compounds **1-hex** and **1**/**2-F** are fluorescent under irradiation with a UV lamp and exhibit moderately efficient (35–45%) fluorescence quantum yields; in contrast, the cyano substituted compounds

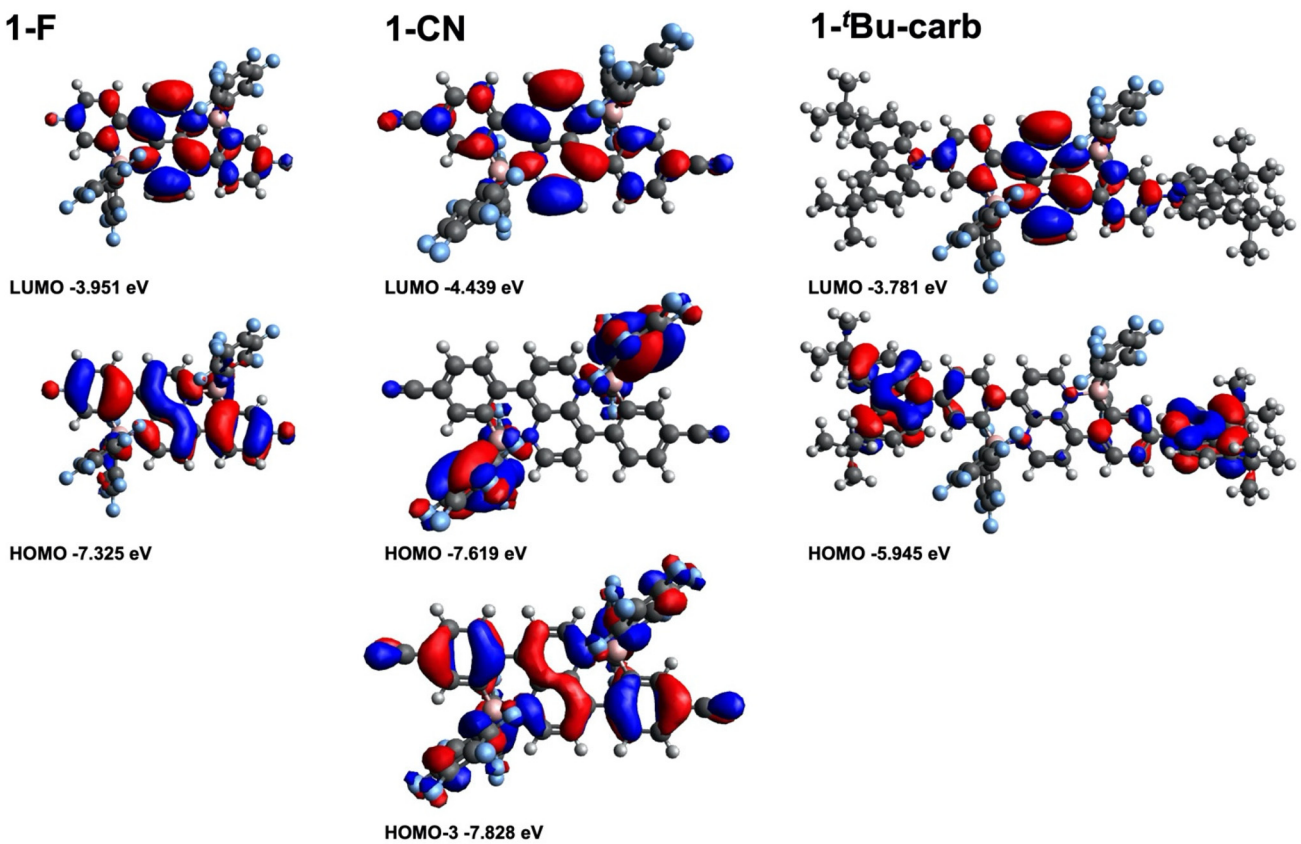

Fig. 7 Representative DFT (PBE0/Def-TZVP)-optimized structures, orbital plots with isosurface values of 0.02 and energy levels (eV) for **1-F**, **1-CN** and **1-^{t}Bu-carb**.

1/2-CN exhibit much lower quantum yields of 3–8% in comparison. This may be due to the weaker absorbance intensity (ε is an order of magnitude lower for these derivatives than the other three,[49] Table 2) or the fact that the π–π* absorbance is actually of HOMO−3 → LUMO character. As shown in Fig. 7, which depicts representative frontier molecular orbitals for **1-F**, **1-CN** and **1-^{t}Bu-carb**, the upper occupied orbitals of **1-CN** (exemplified in the figure by the HOMO) are comprised primarily of the π system on the C_6F_5 substituents on the boron atoms. The first occupied π orbital is the HOMO−3 orbital and is reasonably close in energy to the others. This higher energy π–π* transition is likely the origin of fluorescence in these compounds, and may be partially quenched by the charge transfer HOMO → LUMO absorption (Fig. S15 and S16†).[50] Similarly, the carbazole substituted examples **1/2-^{t}Bu-carb** exhibit no photoluminescent behavior; the HOMO in these complexes (as demonstrated by the electrochemical data discussed above and shown in Fig. 7) is associated with the carbazole nitrogen heterocycle, resulting in much lower energy charge transfer absorbances (see Fig. 8 and Fig. S17 and S18†). In keeping with this assignment, this low energy absorbance exhibits significant solvatochromism in both compounds (Fig. S19–S21†). The significantly lower intensity of this band in **2-^{t}Bu-carb** *vs.* **1-^{t}Bu-carb** is rooted in the positional effect on the conjugation of the carbazole unit with the hexacyclic core of the molecules. In any case, the π orbital of the hexacyclic core in the **1/2-^{t}Bu-carb** derivatives is much lower in energy and fluorescence originating from the π–π* is thus completely quenched in these compounds.

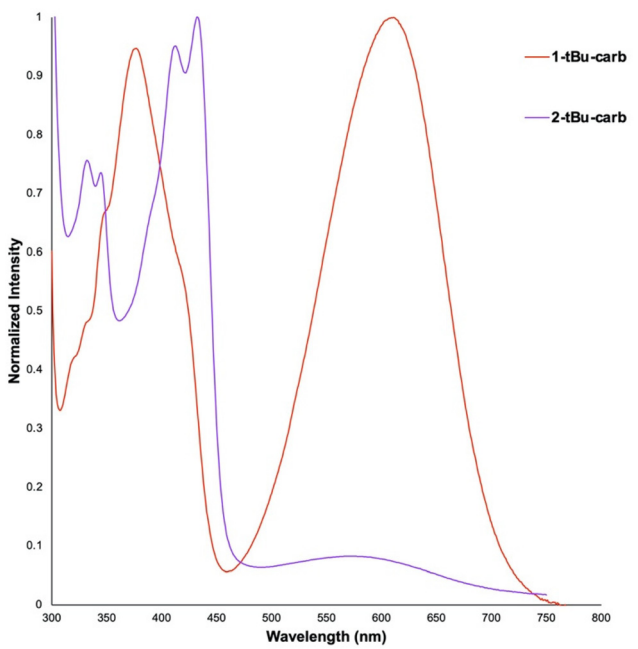

Fig. 8 The absorption spectra of **1-^{t}Bu-carb** (red) and **2-^{t}Bu-carb** (purple). Optical absorption spectra were recorded in 10^{-5} M solutions in DCM.

Conclusions

In conclusion, we have introduced a new borylating reagent, **$(C_6F_5)_2BNTf_2$**, that smoothly introduces $-B(C_6F_5)_2$ units into polycyclic aromatic frameworks *via* pyridyl-directed borylation to provide a facile route to B–N doped organic materials. This was demonstrated using the model substrate 2-phenyl-pyridine, but implemented to prepare a number of examples of a new B–N doped framework, namely the 6a,13a-diaza-7,14-dibora-dibenzo[*a*,*h*]pyrenes. Variation of the donor properties of substituents and their position on the flanking aromatic rings of the hexacyclic core of the molecule gave structurally similar molecules but lead to trends in redox and photophysical behaviour that could be rationalized on the basis of changes to HOMO–LUMO energy gaps and the nature of the transitions in the absorption spectra.

Author contributions

The research was conducted by TN, with preliminary contributions from JLD. The manuscript was prepared by TN and WEP. CYC and WZ performed X-Ray crystallographic analysis on the complexes reported.

Conflicts of interest

There are no conflicts to declare.

Acknowledgements

This research was funded by the Natural Sciences and Engineering Research Council of Canada through a Discovery Grant to WEP. WEP also acknowledges and thanks the Canada Research Chairs program for a Tier I CRC (2020–2027). TN and CYC thanks NSERC for a PGS-D awards.

References

1 G. C. Culling, M. J. S. Dewar and P. A. Marr, *J. Am. Chem. Soc.*, 1964, **86**, 1125–1127.
2 M. J. S. Dewar and R. Dietz, *J. Chem. Soc.*, 1959, 2728–2730, DOI: 10.1039/JR9590002728.
3 M. J. S. Dewar and R. O. Y. Dietz, *J. Org. Chem.*, 1961, **26**, 3253–3256.
4 M. J. S. Dewar, J. Hashmall and V. P. Kubba, *J. Org. Chem.*, 1964, **29**, 1755–1757.
5 M. J. S. Dewar, C. Kaneko and M. K. Bhattacharjee, *J. Am. Chem. Soc.*, 1962, **84**, 4884–4887.
6 M. J. S. Dewar, V. P. Kubba and R. Pettit, *J. Chem. Soc.*, 1958, 3073–3076.
7 M. J. S. Dewar, V. P. Kubba and R. Pettit, *J. Chem. Soc.*, 1958, 3073–3076, DOI: 10.1039/JR9580003073.

8 M. J. D. Bosdet, W. E. Piers, T. S. Sorensen and M. Parvez, *Angew. Chem., Int. Ed.*, 2007, **46**, 4940–4943.
9 Z. Liu and T. B. Marder, *Angew. Chem., Int. Ed.*, 2008, **47**, 242–244.
10 M. J. D. Bosdet and W. E. Piers, *Can. J. Chem.*, 2009, **87**, 8–29.
11 P. G. Campbell, A. J. V. Marwitz and S.-Y. Liu, *Angew. Chem., Int. Ed.*, 2012, **51**, 6074–6092.
12 J. E. Anthony, *Nat. Mater.*, 2014, **13**, 773–775.
13 D. Bonifazi, F. Fasano, M. M. Lorenzo-Garcia, D. Marinelli, H. Oubaha and J. Tasseroul, *Chem. Commun.*, 2015, **51**, 15222–15236.
14 X.-Y. Wang, J.-Y. Wang and J. Pei, *Chem. – Eur. J.*, 2015, **21**, 3528–3539.
15 H. Helten, *Chem. – Eur. J.*, 2016, **22**, 12972–12982.
16 M. M. Morgan and W. E. Piers, *Dalton Trans.*, 2016, **45**, 5920–5924.
17 G. Bélanger-Chabot, H. Braunschweig and D. K. Roy, *Eur. J. Inorg. Chem.*, 2017, **2017**, 4353–4368.
18 Z. X. Giustra and S.-Y. Liu, *J. Am. Chem. Soc.*, 2018, **140**, 1184–1194.
19 C. R. McConnell and S.-Y. Liu, *Chem. Soc. Rev.*, 2019, **48**, 3436–3453.
20 S. K. Mellerup and S. Wang, *Trends Chem.*, 2019, **1**, 77–89.
21 S. A. Iqbal, J. Pahl, K. Yuan and M. J. Ingleson, *Chem. Soc. Rev.*, 2020, **49**, 4564–4591.
22 S. Oda and T. Hatakeyama, *Bull. Chem. Soc. Jpn.*, 2021, **94**, 950–960.
23 X.-Y. Wang, F.-D. Zhuang, R.-B. Wang, X.-C. Wang, X.-Y. Cao, J.-Y. Wang and J. Pei, *J. Am. Chem. Soc.*, 2014, **136**, 3764–3767.
24 B. Neue, J. F. Araneda, W. E. Piers and M. Parvez, *Angew. Chem., Int. Ed.*, 2013, **52**, 9966–9969.
25 T. Hatakeyama, S. Hashimoto, T. Oba and M. Nakamura, *J. Am. Chem. Soc.*, 2012, **134**, 19600–19603.
26 F. Liu, Z. Ding, J. Liu and L. Wang, *Chem. Commun.*, 2017, **53**, 12213–12216.
27 K. Liu, Z. Jiang, R. A. Lalancette, X. Tang and F. Jäkle, *J. Am. Chem. Soc.*, 2022, **144**, 18908–18917.
28 M. M. Morgan, M. Nazari, T. Pickl, J. M. Rautiainen, H. M. Tuononen, W. E. Piers, G. C. Welch and B. S. Gelfand, *Chem. Commun.*, 2019, **55**, 11095–11098.
29 T. K. Wood, W. E. Piers, B. A. Keay and M. Parvez, *Angew. Chem., Int. Ed.*, 2009, **48**, 4009–4012.
30 Y.-L. Rao and S. Wang, *Inorg. Chem.*, 2011, **50**, 12263–12274.
31 D. Li, H. Zhang and Y. Wang, *Chem. Soc. Rev.*, 2013, **42**, 8416–8433.
32 T. S. De Vries, A. Prokofjevs, J. N. Harvey and E. Vedejs, *J. Am. Chem. Soc.*, 2009, **131**, 14679–14687.
33 N. Ishida, T. Moriya, T. Goya and M. Murakami, *J. Org. Chem.*, 2010, **75**, 8709–8712.
34 K. Yuan, N. Suzuki, S. K. Mellerup, X. Wang, S. Yamaguchi and S. Wang, *Org. Lett.*, 2016, **18**, 720–723.
35 D. L. Crossley, J. Cid, L. D. Curless, M. L. Turner and M. J. Ingleson, *Organometallics*, 2015, **34**, 5767–5774.
36 W. E. Piers, S. C. Bourke and K. D. Conroy, *Angew. Chem., Int. Ed.*, 2005, **44**, 5016–5036.
37 P. Koelle and H. Noeth, *Chem. Rev.*, 1985, **85**, 399–418.
38 S. Antoniotti, V. Dalla and E. Duñach, *Angew. Chem., Int. Ed.*, 2010, **49**, 7860–7888.
39 D. W. Beh, W. E. Piers, L. Maron, Y. Yang, B. S. Gelfand and J.-B. Li, *Polyhedron*, 2020, **179**, 114410.
40 R. D. Chambers and T. Chivers, *J. Chem. Soc.*, 1965, 3933–3939.
41 W. E. Piers, R. E. V. Spence, L. R. Macgillivray and M. J. Zaworotko, *Acta Crystallogr., Sect. C: Cryst. Struct. Commun.*, 1995, **51**, 1688–1689.
42 H. Amarne, C. Baik, S. K. Murphy and S. Wang, *Chem. – Eur. J.*, 2010, **16**, 4750–4761.
43 A. R. Katritzky and P. Simmons, *J. Chem. Soc.*, 1960, 1511–1516, DOI: **10.1039/JR9600001511**.
44 H. P. Hopkins Jr., D. V. Jahagirdar, P. S. Moulik, D. H. Aue, H. M. Webb, W. R. Davidson and M. D. Pedley, *J. Am. Chem. Soc.*, 1984, **106**, 4341–4348.
45 K.-Y. Wang, C. Chen, J.-F. Liu, Q. Wang, J. Chang, H.-J. Zhu and C. Li, *Org. Biomol. Chem.*, 2012, **10**, 6693–6693.
46 M. Balkenhohl, R. Greiner, I. S. Makarov, B. Heinz, K. Karaghiosoff, H. Zipse and P. Knochel, *Chem. – Eur. J.*, 2017, **23**, 13046–13050.
47 F. Gagnon, V. Tremblay, A. Soldera, M. U. Ocheje, S. Rondeau-Gagné, M. Leclerc and J.-F. Morin, *Mater. Adv.*, 2022, **3**, 599–603.
48 C. R. Mirle, M. Raja, P. Vasudevarao, S. Sankararaman and R. Kothandaraman, *New J. Chem.*, 2020, **44**, 14401–14410.
49 S.-T. Huang, Y.-C. Hsu, Y.-S. Yen, H. H. Chou, J. T. Lin, C.-W. Chang, C.-P. Hsu, C. Tsai and D.-J. Yin, *J. Phys. Chem. C*, 2008, **112**, 19739–19747.
50 N. Rehmat, A. Toffoletti, Z. Mahmood, X. Zhang, J. Zhao and A. Barbon, *J. Mater. Chem. C*, 2020, **8**, 4701–4712.